Synthesis of Ag-modified ZnO/MWCNT nanoparticles and their application as a catalyst in the degradation of methylene blue

E. M. López Alejandro[a], E. Ramírez Morales[a], M. C. Arellano Cortaza[a], J. P. Morán Lázaro[b], G. Pérez Hernández[a], L. Rojas Blanco[a,*]
[a]*Juárez Autonomous University of Tabasco, Avenida Universidad S/N, Col. Magisterial, Villahermosa, Tabasco. CP. 86040 México.*
[b]*University of Guadalajara de Guadalajara, Los Valles University Center (CUValles), Carretera Guadalajara - Ameca Km. 45.5, 46600, Ameca, Jalisco, México.*

Ag-ZnO/MWCNT composites were obtained by microwave-assisted, varying-charge synthesis of multiwalled carbon nanotubes (MWCNT). The structural, morphological and optical properties were characterized by: XRD, SEM, TEM, Physisorption of N_2 and UV-Vis. The incorporation of Ag ions and MWNTC caused changes in the structure tension and in the average crystallite size of ZnO. The micrographs revealed that ZnO agglomerates were distributed on the MWNTC and that Ag particles were deposited on the surface of the heterostructure, thus the energy gap decreased. The percentages of degradation of methylene blue were 98 and 75% under ultraviolet and visible radiation, respectively, in the Ag-ZnO/CNT composites.

(Received May 12, 2023; Accepted August 4, 2023)

Keywords: Semiconductor, Carbon nanotubes, Doping, Photocatalysis, Organic dyes

1. Introduction

Industrial development benefits many sectors such as the social and economic ones, however, the waste from chemical processes is mostly harmful to the environment [1]. Some examples of harmful substances are recalcitrant molecules with functional groups carboxyl, amino and azo groups; derived from the textile, agricultural, pharmaceutical industry, etc. [2]–[4]. For the elimination of these compounds, various techniques have been used, such as the use of membranes [5], activated carbon [6] and biological processes [7]. Unfortunately, such processes are ineffective in completely removing contaminants. Currently, various studies have found that advanced oxidation processes (AOP's) generate chemical species that transform contaminant molecules into other less complex molecules, even causing their mineralization [8].

Semiconductor-based photocatalysis is part of these mechanisms for the removal of pollutants from effluents [9], [10]. This process begins when electrons are excited in the valence band (VB) with energy greater than the bandgap (E_g) and the electrons are transported to the conduction band (CB) of the material. The photogenerated charges interact with the de H_2O and O_2 molecules adsorbed on the photocatalyst, generating reactive species, such as hydroxyl ions and superoxides, which are responsible for degrading the pollutant molecules [11]. ZnO is a widely used semiconductor in PAOs due to its high chemical stability, its electronic mobility (60 meV) and its non-toxicity [10], [12], [13]. The disadvantages of ZnO are the energy gap, Eg=3.2 eV so it is only photoexcited by ultraviolet (UV) light, which represents about 4% of the total sunlight [14].

Different studies have been focused on modifying the properties of ZnO with dopants that allow the absorption of visible light. Hashim et al.[15] synthesized ZnO and Ag-ZnO nanoparticles by the conventional hydrothermal method. They reported that Ag-doped ZnO is favorable for maxilon blue dye degradation, since impurities promote charge separation compared to pure ZnO.

* Corresponding author: lizethrb@gmail.com
https://doi.org/10.15251/DJNB.2023.183.941

Nada et al., used electrospinning and atomic layer deposition for the doping of ZnO with Pd. In this work, Pd increased the photocurrent in the electrode and ~72% TOC removal was achieved after 240 min of photoelectrocatalytic degradation of paracetamol [16]. Jiang synthesized Cu-ZnO particles by hydrothermal method; the results demonstrated the synergistic effect of the impurities. In addition, the formation of the p-n heterojunction causes a high photocatalytic activity, delays the recombination of the e^-/h^+ pairs and a higher rate of charge carriers participate in the redox reactions [17]. On the other hand, compounds of ZnO and carbon nanotubes [18], graphene [19] and carbon quantum dots [20] have also been reported. CNTs have a high specific surface area, good chemical stability and a high adsorption capacity [21], so they have a wide potential for photocatalytic applications [22], [23]. In many studies, photocatalysts are obtained by long reaction pathways at high temperatures, however it is a priority to reduce these synthesis times using less explored sol-gel synthesis methods. In this work, the structural and optical properties of ZnO particles and Ag-ZnO/CNT composites obtained by microwave-assisted synthesis in short reaction times are analyzed; in addition to the influence on the photocatalytic activity using methylene blue.

2. Experimental

The reagents used in the synthesis process are zinc acetate dihydrate (Zn $(CH_3COO)_2{\cdot}2H_2O$, 99%, Sigma Aldrich), silver nitrate ($AgNO_3$, 99%, CIVEQ), sodium hydroxide (NaOH, 97%, CIVEQ), ethanol (C_2H_5OH, 99.5%, Meyer), deionized water (DI water) and methylene blue (MB, $C_{16}H_{18}ClN_3S$, 98.5%, CIVEQ). Multiple-Walled Nanotubes (MWCNT's), with a diameter of 20-50 nm, were obtained by the synthesis process reported by Alonso-Nuñez et al. [24].

2.1. ZnO synthesis

ZnO particles were synthesized using a 0.48 M solution of Zn $(CH_3COO)_2{\cdot}2H_2O$) in 50 mL of C_2H_5OH and 740 mL of deionized water. The initial pH = 8 was adjusted with NaOH M solution, and the mixture was stirred in ultrasonic for 30 minutes [25]. The microwave was used at 400 W power for 15 min. Subsequently, the supernatant was removed and the solid obtained was washed (H_2O DI) and dried at 120°C for 12 hours.

2.2. Synthesis of Ag-ZnO/MWCNT nanocomposites

The MWCNT's were functionalized using a mixture of concentrated H_2SO_4 and HNO_3 with a 1:1 volume ratio and heating up to 240°C for 6 hours, as indicated in [26], [27]. Finally, the material is washed and dried. To synthesize Ag-ZnO/CNT nanocomposites, a pH=8 solution of $AgNO_3$ (2.2 mM) was prepared and different amounts of MWCNT (6 and 12 mg) were added. The samples obtained are identified as ZnO, Ag-ZnO/6CNT and Ag-ZnO/12CNT.

2.3. Characterization

The materials were structurally characterized by XRD with a Bruker D2 Phaser Rigaku Smartlab diffractometer (Cu Kα= 1.542Å), for the morphological analysis by Scanning Electron Microscopy, a JEOL JSM-7401F, 5 kV and Transmission Electron Microscopy with JEOL were used. JEM-220FS, STEM mode. For the physisorption of N_2, a Quantachrome, Autosorb-iQ2 and optical analysis with a SHIMADZU model UV-2600 spectrophotometer were used.

For the photocatalytic activity, 80 mL of a methylene blue (MB) solution at 10 ppm and 24 mg of photocatalyst were used. A 30 W UV lamp (λ=365 nm) and a complete reflection solar simulator with a 500 W Xenon lamp (Sciencetech, SS0.5KW-A-2-Q) were used.

3. Results and discussion

Fig. 1-a) shows the diffractograms of the synthesized samples, with crystallographic planes associated with the hexagonal wurtzite structure of ZnO (JCPDS 36-1451). In the Ag-ZnO/6CNT and Ag-ZnO/12CNT samples, two peaks of the metallic phase of silver (JCPDS 04-0783) are observed, located at 38.07° and 44.22° of the (111) and (200) crystallographic planes, respectively. These are indicated (*) in the diffractograms. In Fig. 1-b) the planes (100), (002) and (101) of the ZnO in the wurtzite phase are shown, however, in the Ag-ZnO/CNT composites shifts to the left are observed, which are associated to the interstitial incorporation of Ag ions [27], [28]. Therefore, the intensity and width of the ZnO peaks were modified. No signs of NTC's were observed, due to the low amount of material used for their formation.

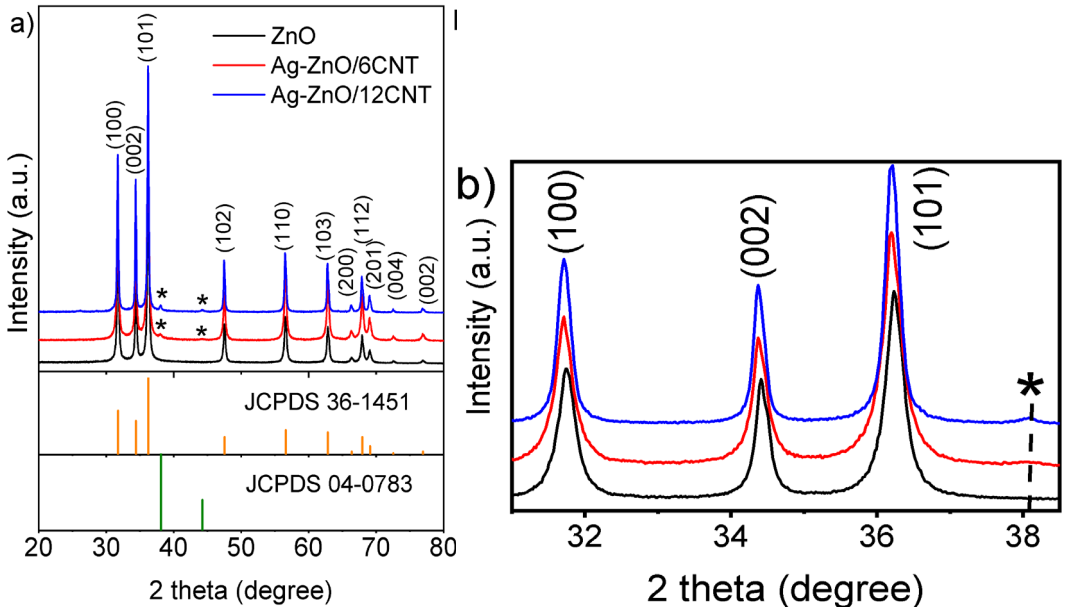

Fig. 1. a) XRD patterns of the synthesized samples, b) Displacement of the ZnO peaks with the incorporation of Ag in the ZnO structure and c) plane (002) corresponding to the MWCNT's.

The crystallite size was calculated with the Debye-Scherrer (D-S) equations (Eq. 1) and the Uniform Strain Model (UDM) of the Williamson Hall (W-H) analysis (Eq. 2):

$$D = \frac{k\,\lambda}{\beta \cos\theta} \tag{1}$$

$$\beta \cos\theta = \frac{k\lambda}{D} + 4\varepsilon \sin\theta \tag{2}$$

where D is the crystallite size, k is a shape factor (~ 0.9), λ is the X-ray wavelength, β is the full width at half maximum (FWHM) of the considered diffraction peak in radians, θ is the Bragg angle and ε is the lattice tension.

For the UDM analysis ($\beta\cos\theta$ vs $4\sin\theta$) the slope was used to calculate the lattice tension and the intercept on the ordinate axis to calculate the average sizes of ZnO crystallites [29]. In addition, the lattice parameters for the ZnO crystals were calculated using Eq 3, 4 (See Table 1).

$$a = \frac{\lambda}{\sqrt{3}\sin\theta_{100}} \tag{3}$$

$$c = \frac{\lambda}{\sin\theta_{002}} \tag{4}$$

Table 1. Parameters calculated for ZnO crystals.

Sample	Crystallite size (nm)		Lattice parameters		dislocation density, δ (nm^{-2})		Strain, ε
	D-S	**W-H**	***a***	***c***	**D-S**	**W-H**	
ZnO	25	66	3.2599	5.2108	0.0016	0.0002	0.0020
Ag-ZnO/6CNT	25	56	3.2628	5.2157	0.0016	0.0003	0.0019
Ag-ZnO/12CNT	32	101	3.2625	5.2171	0.0010	0.0001	0.0018

Table 1 shows that the lattice parameters in ZnO were modified, which is attributed to the difference in ionic radius of Ag^{+} (1.14 Å) and Zn^{2+} (0.74 Å) [30], as shown in Table 1. The number of vacancies and defects in ZnO crystals (δ) was calculated using Eq. 5 [31], where D is the crystallite size.

$$\delta = \frac{1}{D^2} \tag{5}$$

Fig. 2 a-b) shows that δ, compared to pure ZnO, increases when MWCNT's and Ag ions are incorporated, however, an increase in the percentages of MWCNT's causes a significant decrease. The tension in the ZnO lattice decreased quasilinearly with increasing amount of MWCNT's (Fig. 2-c), this can be attributed to the formation of new Zn-O-C and Ag bonds in the nanocomposites [32].

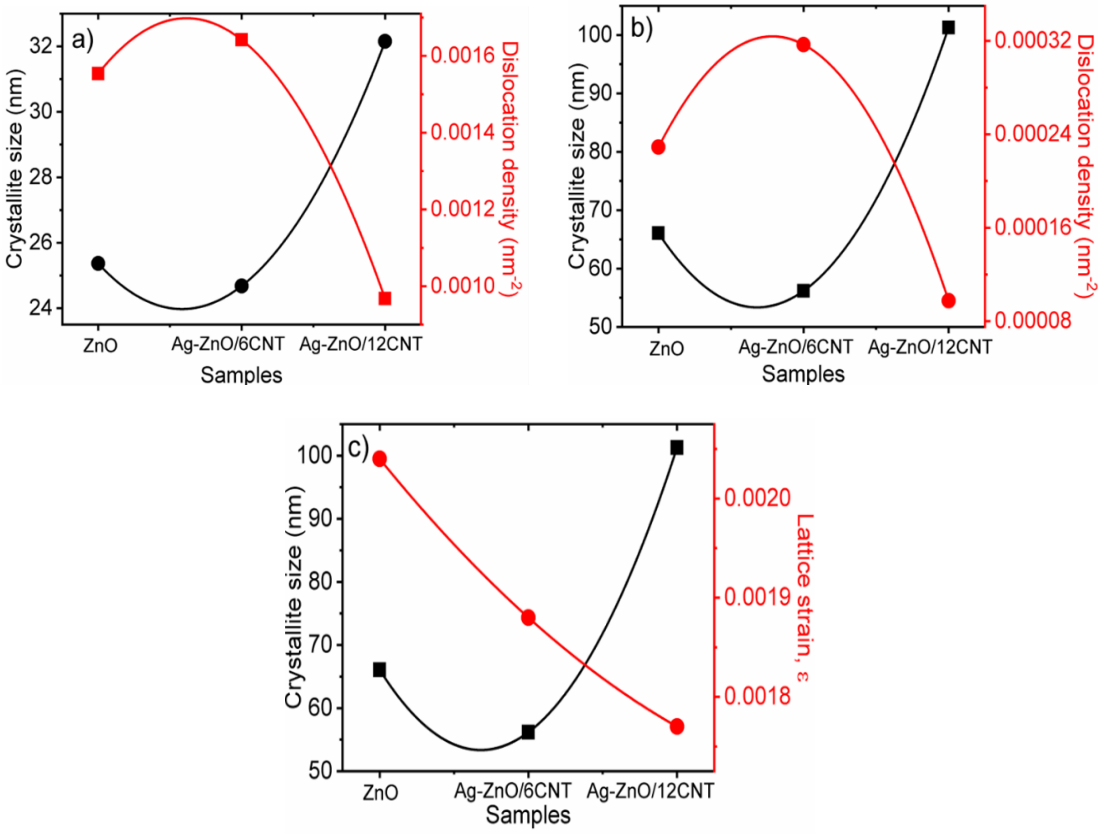

Fig. 2. Plots of crystallite size and dislocation of ZnO nanoparticles using a) D-S analysis and b) W-H analysis. c) Plot of crystallite size and lattice tension of ZnO nanoparticles using W-H analysis.

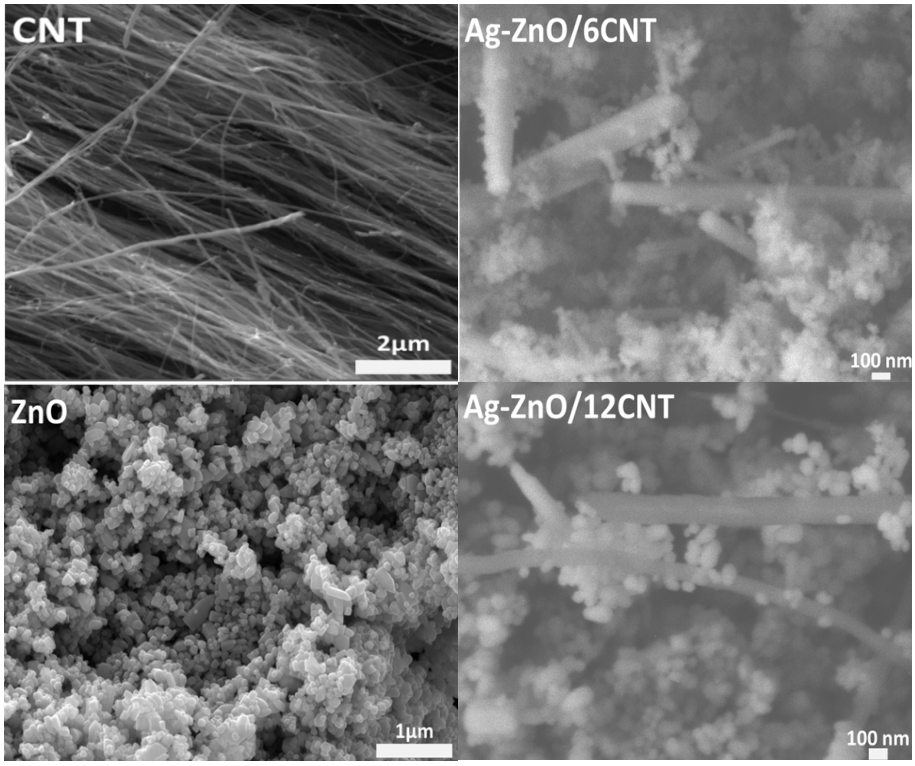

Fig. 3. Micrographs of CNT, ZnO and Ag-ZnO/CNT composites.

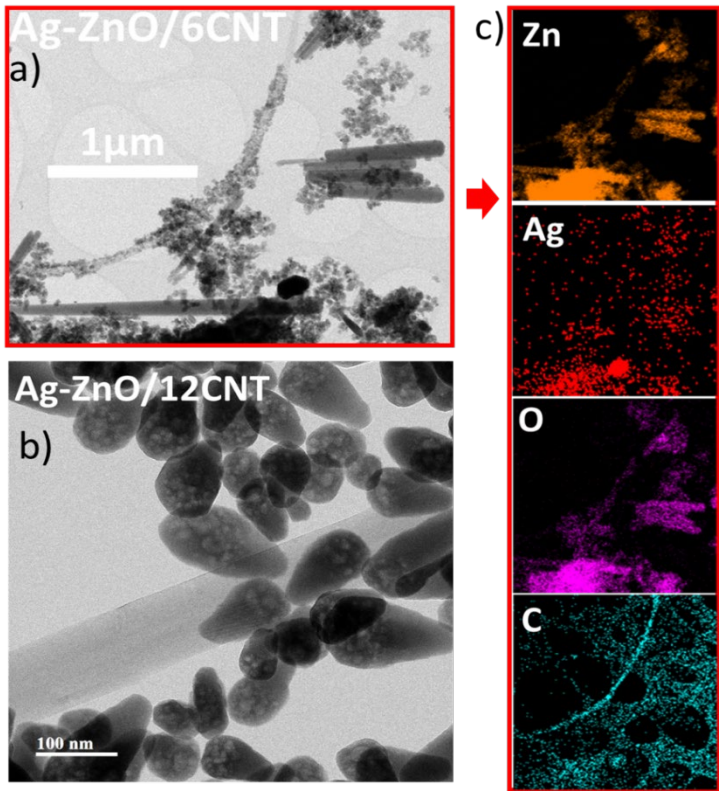

Fig. 4. TEM micrographs of: a) Ag-ZnO/6CNT, b) Ag-ZnO/12CNT and c) EDS analysis of the Ag-ZnO/6CNT sample.

The SEM images of the CNT's, ZnO, and the Ag-ZnO/CNT composites are shown in Fig. 3. In the ZnO micrograph, various conglomerates with an average size of 180 nm are observed. In the micrographs of Ag-ZnO/6CNT and Ag-ZnO/12CNT, a combination of morphologies with the presence of agglomerates distributed around the MWCNTs is observed. Ag particles cannot be seen.

Fig. 4 shows the TEM micrographs of the samples a) Ag-Zn/6CNT and b) Ag-Zn/12CNT, confirming that the ZnO particles are surrounding the MWCNTs. The darkest areas in the micrographs are associated with Ag particles. These results indicate that Ag is found on the surface and not only in the interstices of the ZnO lattice, which increases light absorption [33]. In EDS spectra of the compound Ag-ZnO/6CNT (Fig. 4-c) Zn, Ag, O and C were identified.

Fig. 5 of the absorbance spectra shows the absorption edge of ZnO, located at ~380 nm [34]. The presence of an absorption edge ~430 nm is associated with the surface plasmon resonance (SPR) absorption of Ag nanoparticles, produced by the transfer of photogenerated electrons on the surface of the nanoparticles to the conduction band of the Ag nanoparticles. ZnO [33]. This contributes to improving the photocatalytic efficiency.

On the other hand, the absorption of the Ag-ZnO/12 CNT sample is higher at wavelengths >400 nm, which is attributed to the high sensitivity of MWCNTs to visible light [35].

The bandgap energy were calculated using Eq. 6 [36]:

$$E_g = \frac{1239.84 \times m}{-b} \tag{6}$$

m and b are the slope and y-intercept of the linear fits (Inset Fig. 5). The values of E_g obtained for ZnO, Ag-ZnO/6CNT and Ag-ZnO/12CNT were 3.15, 3.14 and 3.08 eV, respectively. This is attributed to the presence of silver particles on the ZnO surface and the MWNCT´s increase the conductivity in the heterojunction formed with Ag-ZnO [37].

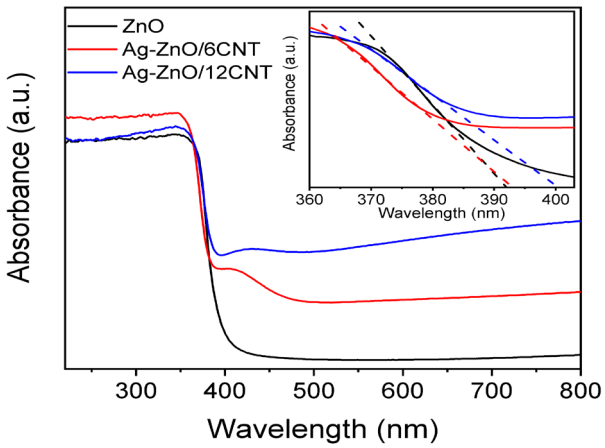

Fig. 5. Absorption spectra of ZnO and Ag-ZnO/CNT compounds. Inset: Fits of the linear portions of the absorbance spectra (R2 ≥ 0.997).

The N_2 adsorption-desorption isotherms are shown in Fig. 6. According to IUPAC, the isotherms of the samples are type IV, with hysteresis loop H3, which are associated with aggregates in laminar form [38]. In the Ag-ZnO/CNT sample, a change in the shape and size of the hysteresis loop is observed, this is associated with the growth of Ag particles on the surface and in the ZnO pores. This is confirmed by the EDS results and by the pore size distribution presented in the insert of Fig. 6.

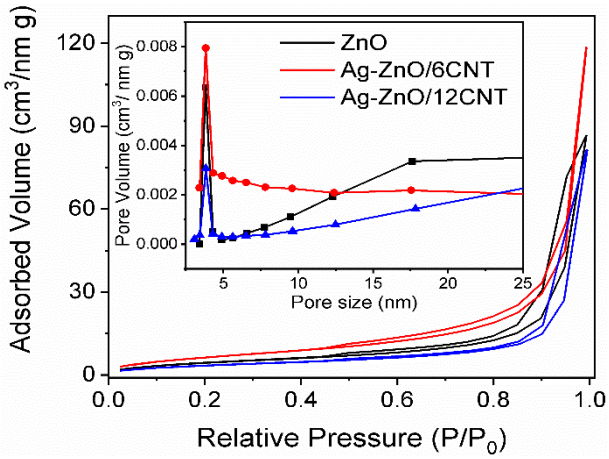

Fig. 6. Nitrogen adsorption-desorption isotherms and pore size distribution curves (Inset).

Specific surface area and pore size distribution were estimated using the BET and BJH methods of adsorption isotherm, respectively. Table 2 shows that the sample with the highest specific surface area is Ag-ZnO/6CNT, so the photocatalytic activity improves by having a greater number of contaminating molecules in contact with the surface of the material. On the other hand, the average pore size is the same in all samples.

Table 2. Textural properties of ZnO and Ag-ZnO/CNT particles.

Sample	BET Area (m^2/g)	Pore diameter (nm)	Pore volume (cc/g)
ZnO	17.08	3.81	0.137
Ag-ZnO/6CNT	25.32	3.82	0.185
Ag-ZnO/12CNT	13.60	3.82	0.127

The solution was first sonicated in the dark for 30 min for adsorption-desorption equilibrium. Subsequently, the photocatalytic degradation of the main band of MB (~665 nm) was evaluated, during a period of 270 minutes. The absorbance spectra (Fig. 7) show a decrease in the MB band with increasing irradiation time and contact with the compounds a) Ag-ZnO/12CNT and b) Ag-ZnO/6CNT. The graphs of $C\ vs\ t$ revealed that the light sources used in the tests do not modify the contaminant molecule, so the observed changes are attributed to the photocatalysts used. To calculate the percentage of degradation ($\%D$) the equation was used [39]:

$$\%D = \frac{A_0 - A_t}{A_0} * 100 \tag{7}$$

where A_0 is the initial absorbance and A_t is the absorbance at time t (See Table 3).

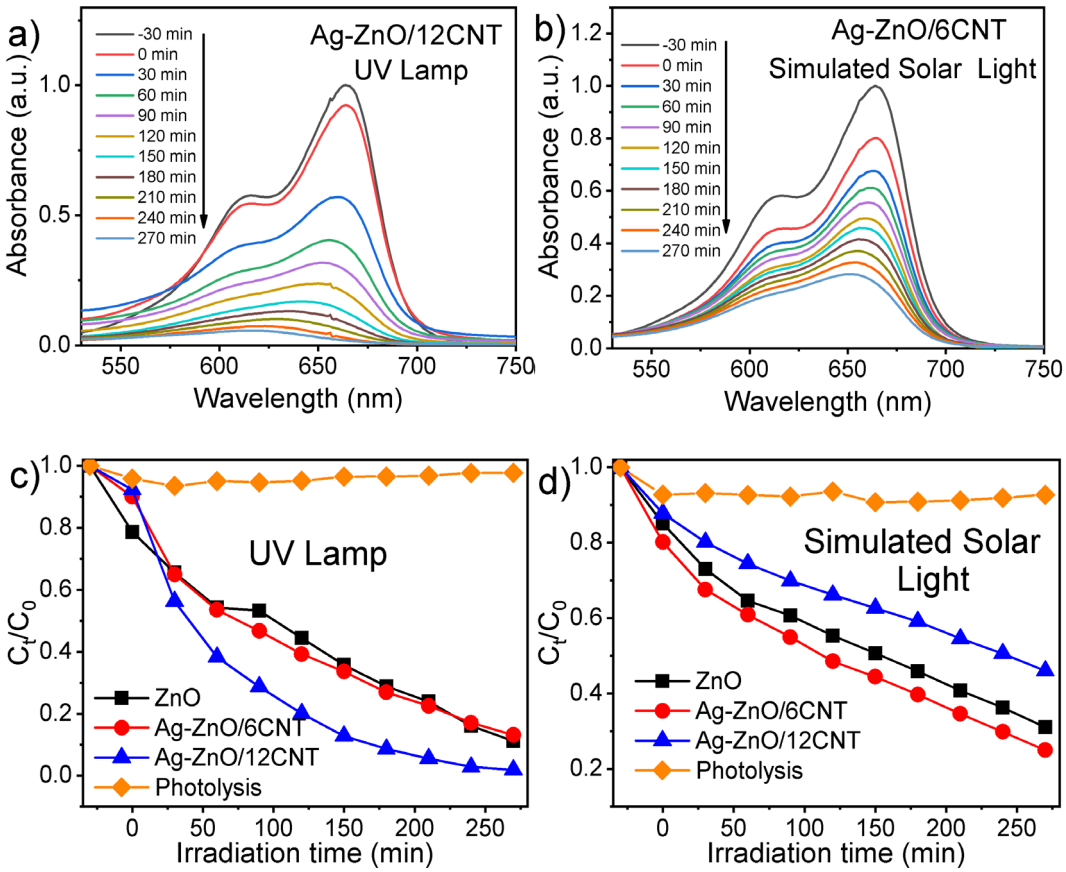

Fig. 7. MB absorbance spectra using a) Ag-ZnO/12CNT in UV light and b) Ag-ZnO/6CNT in visible light. Plots of C vs t of the photocatalysts using: c) UV light and d) simulated sunlight.

Table 3. Summary of photocatalytic performance of ZnO particles and Ag-ZnO/CNT composites under UV and Visible irradiation.

Sample	% D MB	
	UV Lamp	**Simulated Solar Light**
ZnO	89	69
Ag-ZnO/6CNT	87	75
Ag-ZnO/12CNT	98	54

In the tests with UV light and simulated sunlight, the Ag-ZnO/CNT composites showed a higher photocatalytic performance, this is attributed to the increase in the specific surface area, the decrease in the energy gap and the effect of the Ag surface plasmon.

On the other hand, it was shown that the specific surface area decreases when the MWCNT's load increases, however the Ag-ZnO/12CNT sample reached a higher percentage of degradation. The foregoing indicates that even when MWCNTs increase energy absorption in the visible region, a saturation state prevents an improvement in photocatalytic activity, the elimination of O vacancies in the ZnO structure, by the formation of new bonds in the Zn-O-C heterojunction [40, 41].

4. Conclusions

In this work, ZnO particles and Ag-ZnO/CNT heterostructures were successfully synthesized using the microwave-assisted technique. It was determined that the addition of silver promoted changes in the structure of ZnO and the absorption of visible light due to the surface plasmon effect. Also, the incorporation of MWCNT's promoted charge separation and increased the specific surface area in the Ag-ZnO/6CNT composites, improving the photocatalytic activity of MB with simulated sunlight.

Acknowledgements

E. M. López-Alejandro acknowledges CONACyT, Mexico, for financial support through the fellowship.

References

[1] L. Bilińska and M. Gmurek, Water Resour. Ind., vol. 26, 100160(2021); https://doi.org/10.1016/j.wri.2021.100160

[2] P. Katapodis, M. Moukouli, and P. Christakopoulos, Int. Biodeterior. Biodegradation, vol. 60, no. 4, 267(2007); https://doi.org/10.1016/j.ibiod.2007.04.002

[3] B. A. Marinho, L. Suhadolnik, B. Likozar, M. Huš, Ž. Marinko, and M. Čeh, " J. Clean. Prod., vol. 343, 131061(2022); https://doi.org/10.1016/j.jclepro.2022.131061

[4] S. Nanjani et al., Environ. Res., vol. 212, 113288(2022); https://doi.org/10.1016/j.envres.2022.113288

[5] G. Gan, S. Fan, X. Li, Z. Zhang, and Z. Hao, J. Environ. Sci., (2022); https://doi.org/10.1016/j.jes.2022.02.006

[6] X. Liu, H. Zhu, W. Wu, D. Lin, and K. Yang, J. Hazard. Mater., vol. 424, 127355(2022); https://doi.org/10.1016/j.jhazmat.2021.127355

[7] E. Ferrer-Polonio, J. Fernández-Navarro, M.-I. Iborra-Clar, M.-I. Alcaina-Miranda, and J. A. Mendoza-Roca, J. Environ. Manage., vol. 263, 110368(2020); https://doi.org/10.1016/j.jenvman.2020.110368

[8] Q. Q. Cai, L. Jothinathan, S. H. Deng, S. L. Ong, H. Y. Ng, and J. Y. Hu, Advanced Oxidation Processes for Effluent Treatment Plants, Elsevier, 2021, pp. 199-254; https://doi.org/10.1016/B978-0-12-821011-6.00011-6

[9] W. Gao et al., Nano Energy, vol. 71, 104624(2020); https://doi.org/10.1016/j.nanoen.2020.104624

[10] M. L. A. Kumari, L. G. Devi, G. Maia, T.-W. Chen, N. Al-Zaqri, and M. A. Ali, Environ. Res., vol. 203, 111841(2022); https://doi.org/10.1016/j.envres.2021.111841

[11] G. S. Arcanjo, A. H. Mounteer, C. R. Bellato, L. M. M. da Silva, S. H. Brant Dias, and P. R. da Silva, J. Environ. Manage., vol. 211, 154(2018); https://doi.org/10.1016/j.jenvman.2018.01.033

[12] B. Janani et al., J. Taiwan Inst. Chem. Eng., vol. 133, 104271(2022); https://doi.org/10.1016/j.jtice.2022.104271

[13] K. Shahzad et al., J. Mol. Liq., vol. 356, 119036(2022); https://doi.org/10.1016/j.molliq.2022.119036

[14] Y. Liu, C. Xu, Z. Zhu, J. Lu, A. G. Manohari, and Z. Shi, Mater. Res. Bull., vol. 98, 64(2018); https://doi.org/10.1016/j.materresbull.2017.09.057

[15] F. S. Hashim, A. F. Alkaim, S. J. Salim, and A. H. O. Alkhayatt, Chem. Phys. Lett., vol. 737, 136828(2019); https://doi.org/10.1016/j.cplett.2019.136828

[16] A. A. Nada et al., Appl. Mater. Today, vol. 24, 101129(2021); https://doi.org/10.1016/j.apmt.2021.101129

[17] J. Jiang, Z. Mu, H. Xing, Q. Wu, X. Yue, and Y. Lin, Appl. Surf. Sci., vol. 478, 1037(2019); https://doi.org/10.1016/j.apsusc.2019.02.019
[18] M. Ni et al., Microchem. J., vol. 178, 107410(2022); https://doi.org/10.1016/j.microc.2022.107410
[19] M. Kheirabadi et al., J. Colloid Interface Sci., vol. 537, 66(2019); https://doi.org/10.1016/j.jcis.2018.10.102
[20] A. Velumani, P. Sengodan, P. Arumugam, R. Rajendran, S. Santhanam, and M. Palanisamy, Curr. Appl. Phys., vol. 20, no. 10, 1176(2020); https://doi.org/10.1016/j.cap.2020.07.016
[21] P. O. Agboola, S. Haider, and I. Shakir, Ceram. Int., vol. 48, no. 7, 10136(2022); https://doi.org/10.1016/j.ceramint.2021.12.225
[22] Y. Liu, F. Chen, Q. Li, and H. Bao, Mater. Lett., vol. 210, 23(2018); https://doi.org/10.1016/j.matlet.2017.08.111
[23] M. M. Mohamed, M. A. Ghanem, M. Khairy, E. Naguib, and N. H. Alotaibi, Appl. Surf. Sci., vol. 487, 539(2019); https://doi.org/10.1016/j.apsusc.2019.05.135
[24] G. Alonso-Nuñez, A. M. Valenzuela-Muñiz, F. Paraguay-Delgado, A. Aguilar, and Y. Verde, Opt. Mater. (Amst)., vol. 29, no. 1, 134(2006); https://doi.org/10.1016/j.optmat.2006.03.021
[25] F. Izquierdo De la Cruz et al., Appl. Ecol. Environ. Res., vol. 16, no. 5, 5745(2018); https://doi.org/10.15666/aeer/1605_57455756
[26] M.-H. Hsu and C.-J. Chang, J. Hazard. Mater., vol. 278, 444(2014); https://doi.org/10.1016/j.jhazmat.2014.06.038
[27] M. Ahmad, I. Ahmad, E. Ahmed, M. S. Akhtar, and N. R. Khalid, J. Mol. Liq., vol. 311, 113326(2020); https://doi.org/10.1016/j.molliq.2020.113326
[28] S. Y. Gao, X. X. Jia, S. X. Yang, Z. D. Li, and K. Jiang, J. Solid State Chem., vol. 184, no. 4, pp. 764-769, 2011; https://doi.org/10.1016/j.jssc.2011.01.025
[29] V. Mote, Y. Purushotham, and B. Dole, J. Theor. Appl. Phys., vol. 6, no. 1, 2(2012); https://doi.org/10.1186/2251-7235-6-6
[30] K. Ravichandran, R. Uma, S. Sriram, and D. Balamurgan, Ceram. Int., vol. 43, no. 13, 10041(2017); https://doi.org/10.1016/j.ceramint.2017.05.020
[31] S. Mustapha et al., Adv. Nat. Sci. Nanosci. Nanotechnol., vol. 10, 4(2019); https://doi.org/10.1088/2043-6254/ab52f7
[32] M. Mujahid, Bull. Mater. Sci., vol. 38, no. 4, 995(2015); https://doi.org/10.1007/s12034-015-0929-5
[33] G. Kanimozhi, S. Vinoth, H. Kumar, E. S. Srinadhu, and N. Satyanarayana, J. Electron. Mater., vol. 48, no. 7, 4389(2019); https://doi.org/10.1007/s11664-019-07199-2
[34] M. Z. Toe et al., J. Lumin., vol. 229, 117649(2021); https://doi.org/10.1016/j.jlumin.2020.117649
[35] M. Moradi, M. Haghighi, and S. Allahyari, Process Saf. Environ. Prot., vol. 107, 414(2017); https://doi.org/10.1016/j.psep.2017.03.010
[36] R. López and R. Gómez, J. Sol-Gel Sci. Technol., vol. 61, no. 1, 1(2012); https://doi.org/10.1007/s10971-011-2582-9
[37] X. Yan, D. Pan, Z. Li, B. Zhao, J. Zhang, and M. Wu, Mater. Lett., vol. 64, no. 15, 1694(2010); https://doi.org/10.1016/j.matlet.2010.05.009
[38] A. P. Shah, S. Jain, V. J. Mokale, and N. G. Shimpi, J. Ind. Eng. Chem., vol. 77, 154(2019); https://doi.org/10.1016/j.jiec.2019.04.030
[39] M. A. Alvi, A. A. Al-Ghamdi, and M. ShaheerAkhtar, Mater. Lett., vol. 204, 12(2017); https://doi.org/10.1016/j.matlet.2017.06.005
[40] R. V Hariwal, H. K. Malik, A. Negi, and K. Asokan, Appl. Surf. Sci. Adv., vol. 7, 100189(2022); https://doi.org/10.1016/j.apsadv.2021.100189
[41] A. Zaidia, K. Tiwaria, R. R. Awasthib, and K. C. Dubeyc, Chalcogenide Lett., vol. 20, no. 1, 33-41(2023); https://doi.org/10.15251/CL.2023.201.33